Neutron-deuteron scattering calculations with the Paris potential using the W-matrix representation of the two-body input

Th. Januschke, T. N. Frank, and W. Sandhas
Physikalisches Institut, Universität Bonn, D-5300 Bonn 1, Germany

H. Haberzettl
Center for Nuclear Studies, Department of Physics, The George Washington University, Washington, D.C. 20052
(Received 3 October 1991)

Observables of elastic neutron-deuteron scattering are calculated within the framework of the Alt-Grassberger-Sandhas (AGS) three-nucleon equations. As input we use the separable W-matrix representation of the two-body T matrix of the Paris potential. We present a criterion based on the Schmidt norm of the kernel of the AGS equations to optimize this representation. Comparing with an almost complete set of experimental observables, except for a few observables depending sensitively on input not yet fully optimized in this manner, our results generally show good agreement with the data. We thus corroborate previous findings for semirealistic potentials also for realistic interactions, namely that the W-matrix approach provides a very efficient means of calculating three-nucleon scattering processes. Estimates are given showing that this method requires at least an order of magnitude less computational resources than other solution algorithms, without sacrificing accuracy.

PACS number(s): 13.75.Cs, 25.40.-h

I. INTRODUCTION

In Refs. [1] and [2], it was shown for the semirealistic S-wave Malfliet-Tjon interactions [3] MT I and MT III that the W-matrix formalism of Ref. [4] provides an excellent way of representing the two-body input for neutron-deuteron elastic [1] scattering and breakup [2] calculations. Here, we will present results for elastic neutron-deuteron scattering based on the realistic Paris potential [5] calculated within the framework of the effective two-body formulation of the three-nucleon Alt-Grassberger-Sandhas (AGS) equations [6].

In solving the three-body problem, essentially there exist two strategies. The first, the direct-integration method, is to discretize the partial-wave-decomposed two-dimensional integral equations into finite summations in *both* momentum variables and invert the resulting system of linear equations. The second approach consists of representing the two-nucleon subsystem input in terms of separable expansions of the two-nucleon amplitudes entering the kernel of the AGS equations. In the spirit of the original Fredholm theory of integral equations with degenerate kernels, this corresponds to an explicit partial solution of the two-dimensional integral equation with respect to the subsystem momentum variable. The use of such expansions, therefore, always results in a reduction of the dimensionality of the equations to one-dimensional integral equations in terms of the spectator momentum of the third nucleon relative to the two-nucleon subsystem.

In assessing the merits of the latter approach, it must be emphasized that a separable expansion is not just a convenient representation of the input but a true reflection of the mathematical structure of these subamplitudes. The imaginary part of the two-body T matrix, for example, is completely separable, without any nonseparable remainder; this follows from the unitarity relation. For the real part, the dominant contributions stem from the bound state and resonance poles around which the T matrix possesses a factorizable residue; in other words, these contributions are separable, too. If, therefore, the expansion is chosen such that it reflects the existing separable structures, it is to be expected that the number of required expansion functions will be small enough to provide a considerable saving of computing time *without any loss of numerical accuracy* as compared to a direct two-dimensional integration.

Existing numerical solutions of the AGS equations for nucleon-deuteron scattering with realistic forces employ both strategies: Ref. [7] uses the direct two-dimensional discretization method and Ref. [8] expands the two-body input into a series of separable terms according to the Ernst-Shakin-Thaler (EST) prescription [9]. In the former case [7], the dimension of the resulting kernel matrix is so large that with today's computing facilities the corresponding system of linear equations cannot be inverted directly and one has to revert to an iterative solution in terms of Padé approximants. In the latter case [8], the number of terms required for expanding the Paris potential reliably may be as high as 25 even for uncoupled partial waves (i.e., the approximation is of rank 5).

The W-matrix representation of the two-body T matrix provides an exact splitting of the full T matrix into a separable and a nonseparable part [4]. Its particular usefulness in three-body calculations stems from the fact that it allows one to concentrate in the separable part in an exact manner the *entire* pole and cut contributions of the subsystem. This separable part is of rank 1 for un-

coupled and of rank 2 for coupled partial waves, irrespective of which interaction is used. The corresponding real and nonsingular remainder always vanishes half on shell. The separable part alone, therefore, provides a fully unitary approximate input for three-nucleon equations. Furthermore, in order to optimize this treatment, one still has at one's disposal an open parameter function $k(E_2)$ of the two-body subsystem energy E_2 which may be adjusted to minimize the effect of the neglected remainder. This input to three-nucleon equations, therefore, strikes a balance between simplicity on the one hand and an accurate reflection of the dominant behavior of the exact T matrix on the other. In the latter respect we emphasize that the separable part results from properties of the T matrix itself, and not from some unspecific expansion of the potential. As a consequence, the number of channels is exactly the same as prescribed by the physical quantum numbers, i.e., the separable representation itself does not introduce additional couplings enumerated by expansion indices. Since, moreover, integrations need to be carried out only with respect to one relative momentum (instead of the original two), the resulting system of linear equations is small enough to be solvable without requiring any compromise as to numerical accuracy. The numerical error of our solutions, therefore, is well within 1%.

In Sec. II, we first recapitulate the W-matrix formalism for coupled partial waves, as required for the application to realistic two-body forces. Without going into any details of the derivation, we then write down the three-nucleon AGS equations resulting from the present approach.

From a practical point of view, the optimization of the approximate input by an appropriate choice of $k(E_2)$ plays a very central role in the W-matrix approach. In the previous calculations with semirealistic potentials [1,2] this was achieved rather simply by a variational principle. Since this is no longer possible for realistic interactions, we present in Sec. III a general optimization procedure based on an investigation of contributions to the Schmidt norm of the kernel of the three-nucleon AGS equations. For the present calculations, in view of limited CRAY computing time, we could employ this procedure only for the three-body seven-channel problem. For larger two-body input, we then used the same function $k(E_2)$. (The seven-channel problem refers to a scattering calculation with maximal total angular momentum $\Gamma \geq \frac{3}{2}$ using ${}^1S_0$ and ${}^3S_1-{}^3D_1$ two-body partial-wave input; a three-nucleon bound state calculation with this input is referred to as a five-channel problem since in that case one has only $\Gamma=\frac{1}{2}$.)

In Sec. IV, we compare the numerical results thus obtained with experimental data. In general, we find good agreement with the measured data, except for observables which are known to be very sensitive to the two-body P-wave input, and which is not yet fully optimized in our present numerical treatment. Presenting our conclusions in Sec. V, we argue that the employment of the Schmidt norm optimization procedure for all partial waves, however, will lead to solutions of the three-nucleon equations for realistic potentials which are of the same high quality as those found previously for semirealistic interactions.

II. FORMALISM

The formulas in Ref. [1] were tailored to the fact that the underlying nucleon-nucleon interactions used there acted only in the S waves. In the following we provide all relevant formulas necessary for realistic NN potentials. At first, we recapitulate the W-matrix formalism which provides the two-body input for the three-body AGS equations. We use units in which the nucleon mass is unity, i.e., 41.47 MeV fm^2=1.

A. W matrix

It is a straightforward exercise to extend the W-matrix formalism of Ref. [4] to the case of coupled partial waves. We start by introducing a reduced potential matrix element $U_{ll'}$ for coupled partial waves l and l' by

$$U_{ll'}(p,p')=p^{-l}V_{ll'}(p,p')p'^{-l'} \tag{1}$$

in terms of the partial-wave momentum-space matrix element $V_{ll'}$ of the two-body potential V. The momentum factors p^{-l} and $p'^{-l'}$ are chosen such that $U_{ll'}(p,p')$ does not vanish for vanishing momenta p,p' for $l,l'>0$. (The generalization given in Ref. [10] uses a slightly different, unsymmetric definition for $U_{ll'}(p,p')$. Our present choice follows from practical considerations; it greatly facilitates the numerical treatment of all ensuing expressions for small momenta. As a consequence, also the uncoupled case, which follows by setting $V_{ll'}=\delta_{ll'}V_l$, produces expressions somewhat different from those of Refs. [1, 2, and 4].)

The W matrix $W_{\hat{l}\hat{l}}$ is then defined as the solution of

$$W_{\hat{l}\hat{l}}(p,p';E)=U_{\hat{l}\hat{l}}(p,p';E)+\sum_{l'}\int_0^\infty dq\, q^2\frac{U_{ll'}(p,q;E)-U_{ll'}(p,k;E)}{E-q^2}q^{2l'}W_{l'\hat{l}}(q,p';E)\ . \tag{2}$$

Obviously, because of the subtraction of $U_{ll'}(p,k;E)$ in the kernel, the W matrix is a function of the parameter momentum k; in the notation $W_{\hat{l}\hat{l}}(p,p';E)$ this dependence is suppressed for reasons of a more concise notation. This parameter is to be chosen such that

$$k=\begin{cases}\sqrt{E} & \text{for } E\geq 0\ ,\\ \text{arbitrary} & \text{for } E<0\ .\end{cases} \tag{3}$$

In other words, the integral equation (2) is nonsingular for scattering energies $E\geq 0$. As a consequence, the W

matrices are real functions of the energy even for $E \geq 0$, without any poles and cuts. These analytical properties make them some of the most "benign" functions in potential scattering theory. (For a detailed account of the underlying relations in the case of local potentials, see Ref. [4].) Note that the subtraction in the kernel of (2) also means that $W_{\hat{l}\hat{l}}(p,p';E)$ no longer possesses the usual symmetry properties of the potential, i.e., the analogue of

$$V_{ll'}(p,p') = V_{l'l}(p',p)$$

is not true for $W_{\hat{l}\hat{l}}(p,p';E)$. Furthermore, as will become obvious from the expressions given below, there is an additional asymmetry of $W_{\hat{l}\hat{l}}(p,p';E)$ with respect to its partial-wave indices l and $\hat{l}$. While the former has a direct physical significance, the latter serves only as an internal summation index of the W-matrix representation (to distinguish these indices from true partial-wave indices we will consistently use a caret).

At negative energies, the parameter k is not only arbitrary, it is not even limited to be a constant. It may be any (nonpathological) function of the energy and it may even be chosen to be different for different partial waves, i.e., the k dependence of the subtracted reduced potential in the kernel of (2) is given in detail by

$$U_{ll'}(p,k;E) = U_{ll'}(p,k_{ll'}(E);E) ,$$

which means that, in general, the W-matrix elements $W_{\hat{l}\hat{l}}(p,p';E)$ are functions of $k_{\hat{l}\hat{l}}(E)$. This freedom in choosing k at negative energies will play an important role in the considerations of Sec. III. To simplify the language, we shall refer to $W_{\hat{l}\hat{l}}(p,k;E)$ as the half-on-shell W matrix even if $E<0$ where this, strictly speaking, is not quite appropriate.

Just as in the uncoupled case discussed in detail in Ref. [4], one easily shows now that the solution of the integral equation (2) completely determines the two-body scattering problem also for the coupled case. Instead of solving the singular Lippman-Schwinger (LS) equation,

$$T_{ll'}(p,p';E+i0) = V_{ll'}(p,p') + \sum_{l''} \int_0^\infty dq\, q^2 \frac{V_{ll''}(p,q)}{E+i0-q^2} T_{l''l'}(q,p';E+i0) , \quad (4)$$

one finds that the fully off-shell two-body T matrix $T_{ll'}(p,p';E+i0)$ may be decomposed exactly into a separable term $T^s_{ll'}(p,p';E+i0)$ and a nonseparable, real remainder $R_{ll'}(p,p';E)$,

$$T_{ll'}(p,p';E+i0) = T^s_{ll'}(p,p';E+i0) + R_{ll'}(p,p';E) , \quad (5)$$

both of which are given entirely in terms of the solutions of the nonsingular W-matrix equation (2); i.e.,

$$T^s_{ll'}(p,p';E+i0) = p^l \sum_{\hat{l},\hat{l}'} W_{\hat{l}\hat{l}}(p,k;E)\Delta_{\hat{l}\hat{l}'}(E+i0) \times W_{l'\hat{l}'}(p',k;E)p'^{l'} , \quad (6)$$

and

$$R_{ll'}(p,p';E) = p^l \left[W_{ll'}(p,p';E) - \sum_{\hat{l},\hat{l}'} W_{\hat{l}\hat{l}}(p,k;E) W^{-1}_{\hat{l}\hat{l}'}(k,k;E) W_{\hat{l}'l'}(k,p';E) \right] p'^{l'} . \quad (7)$$

As one immediately verifies by inserting the momentum k for p or p', the remainder $R_{ll'}$ vanishes half on-shell. In other words, the separable part (6) alone provides the full off-shell unitarity relation of the exact T matrix. Since the W matrices are real, the pole and cut structure of the full T matrix is contained solely in the "propagator" $\Delta_{\hat{l}\hat{l}'}(E+i0)$ in Eq. (6),

$$\Delta_{\hat{l}\hat{l}'}(E+i0) = \sum_{\hat{l}''} F^{-1}_{\hat{l}\hat{l}''}(E+i0) W^{-1}_{\hat{l}''\hat{l}'}(k,k;E) , \quad (8)$$

where $F(E+i0)$ is a generalization of the Jost function (or Jost matrix, rather, in the coupled case) given by

$$F_{\hat{l}\hat{l}'}(E+i0) = \delta_{\hat{l}\hat{l}'} - \int_0^\infty dq\, q^2 q^{2\hat{l}} \frac{W_{\hat{l}\hat{l}'}(q,k;E)}{E+i0-q^2} . \quad (9)$$

The generalization concerns only the negative-energy domain and is due to the freedom of choosing the parameter k according to (3); for positive scattering energies, $F(E+i0)$ reduces to the usual Jost function (cf. also discussion in Ref. [4]).

The bound state pole (if it exists) of the T matrix at the energy $E=-\alpha^2$ is contained in the propagator (8); it is identified by the condition

$$\det F(-\alpha^2) = 0 . \quad (10)$$

If this necessary and sufficient condition for the existence of a bound state is met, the Jost matrix cannot be inverted and the eigenvalue equation

$$\sum_{\hat{l}} F_{\hat{l}\hat{l}}(-\alpha^2) C_{\hat{l}} = 0 \quad (11)$$

possesses nontrivial solutions $C_{\hat{l}}$. The properly normalized components ψ_l of the corresponding bound state wave function are then given by linear combinations of the solutions of (2) at the energy $E=-\alpha^2$ according to

$$\psi_l(p) = \frac{p^l}{-\alpha^2-p^2} N \sum_{\hat{l}} W_{\hat{l}\hat{l}}(p,k;-\alpha^2) C_{\hat{l}} , \quad (12)$$

where N is the overall normalization factor determined in the usual way. Despite the formal appearance of the parameter k in (12), these fully normalized bound-state

wave functions are independent of k (as they must be, of course).

These relations provide a complete solution of the off-shell coupled partial-wave two-body problem in terms of the real W matrices (2). In the three-body calculations presented below, we will use the Paris potential [5] as the underlying NN interaction and we will employ the separable part (6) of the corresponding W-matrix representation alone. We emphasize that this approximation of the Paris potential affects only fully off-shell contributions of the two-body interaction (since the separable part is exact half on shell) and that this approximate input satisfies the full off-shell unitarity relation. To optimize this treatment, i.e., to minimize the effect of the neglected remainder (7), we still have at our disposal the free parameter k at negative two-body energies. (Instead of optimizing k, one could also include further separable representations of the remainder according to the prescription of Ref. [4]. Our investigations indicate, however, that first optimizing the lowest-order approximation before adding more terms is far more efficient.)

From Eq. (6) and all related expressions it is obvious that one needs but the half-on-shell solutions $W_{\ell\hat{\ell}}(p,k;E)$ of (2) to carry out this approximation scheme, i.e., only those which are directly, at least formally, related to the bound-state components (12).

As a further technical detail we mention that the representation (5)–(7) is derived under the condition

$$\det W(k,k;E)\neq 0 , \tag{13}$$

i.e., we require that the on-shell W matrix $W(k,k;E)$ may be inverted. For certain simple rank-1 separable potentials this is not true. Since, however, in real applications such potentials presumably would not be subjected anyway to the procedure described here (since they are already separable), we do not consider this a serious problem. For the Paris potential we have observed a violation of (13) for isolated value pairs (k,E) at negative two-body energies E. In these cases the problem can be circumvented rather easily by choosing a different functional form for the parameter k.

B. Three-body AGS equations

For a detailed account of the theory behind the AGS equations, we refer to Ref. [6]. Here, we only give the final form of the effective two-body equations for neutron-deuteron scattering resulting from employing the separable part (6) of the T matrix. (More details of the derivation of the present formulation can be found in Ref. [11].)

Denoting the total angular momentum by Γ and the total isospin by I, the symmetrized partial-wave-decomposed three-nucleon AGS equations read

$$T^{\Gamma I}_{\beta\alpha}(q',q;E+i0)=V^{\Gamma I}_{\beta\alpha}(q',q;E+i0)+\sum_{\mu,\nu}\int_0^\infty dq''q''^2 V^{\Gamma I}_{\beta\mu}(q',q'';E+i0)\Delta_{\mu\nu}(E-\tfrac{3}{4}q''^2+i0)T^{\Gamma I}_{\nu\alpha}(q'',q;E+i0) , \tag{14}$$

where E now denotes the three-body CMS energy. The labels α, β, μ, ν denote sets of quantum numbers comprising spin, angular momentum, and isospin, viz.

$$\beta=\begin{bmatrix}\eta'K'L'\\ \hat{l}'\end{bmatrix} , \quad \alpha=\begin{bmatrix}\eta KL\\ \hat{l}\end{bmatrix} \tag{15}$$

(and analogously for μ, ν). The detailed index structure of $T^{\Gamma I}_{\beta\alpha}$ and $\Delta_{\beta\alpha}$ reads

$$T^{\Gamma I}_{\beta\alpha}\equiv {}^{\Gamma I}T^{\eta'K'L'\eta KL}_{\hat{l}'\hat{l}} \tag{16}$$

and

$$\Delta_{\beta\alpha}\equiv\delta_{\eta'\eta}\delta_{K'K}\delta_{L'L}\Delta^{\eta}_{\hat{l}'\hat{l}} , \tag{17}$$

respectively. The two-body propagators $\Delta^{\eta}_{\hat{l}\hat{l}}$ of Eq. (8) now have acquired an index η which describes the quantum numbers of the two-body subsystem,

$$\eta=\{S,J^\pi;T\} , \tag{18}$$

where S is the spin, J the total angular momentum [with coupling sequence $(l,S)J$], $\pi=(-1)^l$ the parity, and T the isospin of the subsystem. The quantum numbers K and L in (15) describe the channel spin of the three nucleons [with coupling sequence $(J,\frac{1}{2})K$] and the relative angular momentum between the subsystem and the third nucleon, respectively. In other words, the total angular momentum follows from the coupling sequence $(K,L)\Gamma$.

The effective potentials $V^{\Gamma I}_{\beta\alpha}$, with an explicit index structure completely analogous to (16), are given by

$$V^{\Gamma I}_{\beta\alpha}(q',q;E+i0)=2\sum_{l,l'}q'^{l+l'}\sum_{H=0}^{H_{\max}}\left\{\sum_{h=0}^{l+l'}\left[\frac{q}{q'}\right]^h U^{\Gamma I}_{\beta\alpha}(H,h)\right\}\frac{1}{2qq'}\int_{-1}^{+1}dx\, W^{\eta'}_{l'\hat{l}'}(p'_x,k';E'_2)\frac{P_H(x)}{y-x+i0}W^{\eta}_{\ell\hat{l}}(p_x,k;E_2) , \tag{19}$$

where

$$p_x=\sqrt{q'^2+\tfrac{1}{4}q^2+qq'x}\ ,\quad p'_x=\sqrt{q^2+\tfrac{1}{4}q'^2+qq'x} \tag{20}$$

are the two-body subsystem momenta and

$$E_2=E-\tfrac{3}{4}q^2\ ,\quad E'_2=E-\tfrac{3}{4}q'^2 \tag{21}$$

are the two-nucleon energies (denoted by E in Sec. II). Furthermore,

$$y=\frac{E-q^2-q'^2}{qq'} \tag{22}$$

and $P_H(x)$ is the order H Legendre polynomial of the first kind, and

$$H_{\max}=\tfrac{1}{2}(L+l+L'+l')\ . \tag{23}$$

The spin-isospin recoupling coefficients $U^{\Gamma I}_{\beta\alpha}(H,h)$ are given in the Appendix.

As can be seen from (16), the solution of Eq. (14) is not yet the physical (partial-wave) T matrix; one still must sum over the W-matrix indices $\hat{l},\hat{l}'$. The physical matrix element is given by

$${}^{\Gamma I}T^{\eta' K' L' \eta K L}=N^2\sum_{\hat{l},\hat{l}'}{}^{\Gamma I}T^{\eta' K' L' \eta K L}_{\hat{l}'\hat{l}}C_{\hat{l}'}C_{\hat{l}}\ , \tag{24}$$

where the factors are a consequence of the corresponding ones from Eq. (12). Inspection of Eq. (14) shows that the rightmost summation over $\hat{l}$ may be performed already before a numerical solution.

The only transition of physical interest in elastic neutron-deuteron scattering is the one with $\eta=\eta'=d$, where d denotes the deuteron. The full amplitude for the scattering of a neutron with momentum $\mathbf{q}$ and spin component m off a deuteron with total angular momentum component M is given by

$$\langle \mathbf{q}'m'M'|T^{dd}(E+i0)|\mathbf{q}mM\rangle=\sum_{K,M_K}\sum_{K',M'_K}\langle 1M'\tfrac{1}{2}m'|K'M'_K\rangle\langle 1M\tfrac{1}{2}m|KM_K\rangle\langle \mathbf{q}'K'M'_K|T^{dd}(E+i0)|\mathbf{q}KM_K\rangle \tag{25}$$

where

$$\langle \mathbf{q}'K'M'_K|T^{dd}(E+i0)|\mathbf{q}KM_K\rangle=\sum_{L,M_L}\sum_{L',M'_L}\sum_{\Gamma,M_\Gamma}Y_{L'M'_L}(\mathbf{q}')Y^*_{LM_L}(\hat{q})\langle K'M'_K L'M'_L|\Gamma M_\Gamma\rangle\langle KM_K LM_L|\Gamma M_\Gamma\rangle$$
$$\times{}^{\Gamma I}T^{dK'L'dKL}(q',q;E+i0)\ . \tag{26}$$

The Y_{LM} are spherical harmonics and $\hat{q}$ is the direction of the vector $\mathbf{q}$ (similarly for $\mathbf{q}'$); the bras and kets are Clebsch-Gordan coefficients.

III. CHOOSING $k(E_2)$

The first step towards a numerical solution of the three-nucleon equation (14) is the determination of the free parameter k of the W matrices at negative two-body energies such that the influence of the neglected remainder (7) is minimized. In Ref. [1], it was observed that calculating the triton binding energy as a function of k (with k chosen as a constant) exhibited a minimum which coincided with the corresponding exact value of the binding energy. It was conjectured, therefore, that there exists a variational principle which underlies this finding. Furthermore, for the semirealistic MT I and MT III potentials used in Refs. [1] and [2], it was then found that the parameter k corresponding to the minimal binding energy provided scattering results which also were compatible with reference calculations.

In the meantime a proof of the conjectured variational principle was found [12] showing that it is valid for all two-body interactions for which the three-body generalization of the Hilbert-Schmidt expansion [13] is well defined. (Contrary to popular belief, the assumptions underlying a Hilbert-Schmidt expansion of the three-nucleon LS kernel are *not* valid in general. Our experience suggests that more realistic potentials do not admit a well-defined Hilbert-Schmidt expansion.) Numerically, this may be tested very simply by checking whether all eigenvalues of the three-nucleon LS kernel remain real for negative energies. The MT I and MT III potentials used in Refs. [1] and [2] satisfy this criterion and the findings of Ref. [1] for the triton binding energy are, indeed, variational results. (The violation of the conjectured variational principle reported in Ref. [14] was subsequently shown [15] to be in error.)

For the Paris potential, this criterion is not valid (i.e., the higher-order eigenvalues of the LS kernel contain imaginary admixtures) and the variational principle is no longer true. However, from the smallness of the imaginary parts one may infer that the violation to be expected presumably will be rather small. Indeed, using the separable ${}^1S_0$ and ${}^3S_1$-${}^3D_1$ two-body contributions of the Paris potential and employing the variational procedure by separately varying k for ${}^1S_0$ and ${}^3S_1$-${}^3D_1$, numerically we find no violation. Moreover, the minimal triton energy of -7.295 MeV thus found compares very well with the complete five-channel calculations of -7.303 and -7.308 MeV of Refs. [16] and [17], respectively, i.e., the deviation from the complete calculation is less than 0.2%.

However, in the absence of a strict variational principle, this may be just fortuitous and it is, therefore, desirable to have some other means of choosing k. Since constant values for k, albeit different ones in different two-body channels, do not fully exploit the freedom one has, ideally one would like a procedure which yields k as a function of the energy such that the contributions from the remainder (7) are minimized. As a first step in this direction, one may look at the average values of p_x in Eq. (19) as a function of the corresponding two-body energy E_2 (similarly for p_x' and E_2'). Choosing k in $W_{ll}^{\eta}(p_x,k;E_2)$ equal to these average values will ensure that the remainder vanishes on average. Writing explicitly the arguments of the right-most of the two W matrices in Eq. (19), one has with (20) and (21)

$$W_{ll}^{\eta}(p_x,k;E_2)=W_{ll}^{\eta}(\sqrt{q'^2+\tfrac{1}{4}q^2+qq'x}\,,k;E-\tfrac{3}{4}q^2)\ . \tag{27}$$

Using then the fact that on average the contributions due to the x integration in Eq. (19) may be expected to be at $x=0$ and that $E_2=E-\frac{3}{4}q^2$ is the two-body energy belonging to the three-body energy E, one finds that the average value of p_x is given by

$$p_0=\sqrt{q'^2+\tfrac{1}{4}q^2}=\left[\frac{E-E_2}{3}+q'^2\right]^{1/2}\ . \tag{28}$$

A similar result, with q and q' interchanged, is obtained for the leftmost W matrix in Eq. (19). These average contributions will account for most of the subsystem contributions if the remainder vanishes for these momenta. Obviously this is achieved by choosing k as a function of the two-body subsystem energy E_2 in the form

$$k(E_2)=\left[\frac{E_{\rm off}-E_2}{3}\right]^{1/2}\quad \text{for } E_2\le 0\ , \tag{29}$$

where $E_{\rm off}$ is some energy offset which corresponds to averaging in Eq. (28) the different q'^2 for a given three-nucleon energy E. Using this functional form and calculating the triton energy as a function of $E_{\rm off}$, we find the result of Fig. 1 which shows that the minimum energy is now slightly, by about 0.6%, below the reference value from Ref. [17], in violation of the variational principle. One also sees from Fig. 1 that offset values of 15 or 35 MeV will reproduce the reference triton energy of -7.308 MeV.

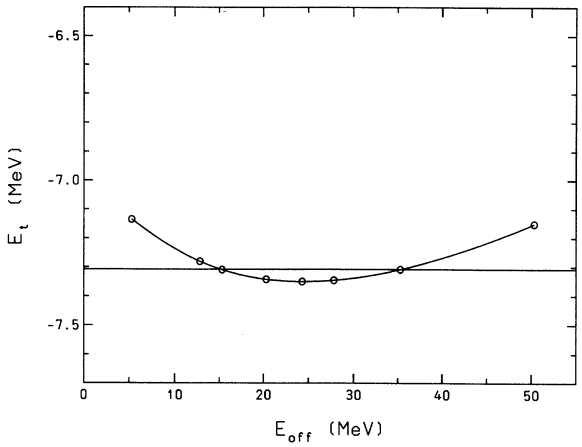

FIG. 1. Results of a five-channel triton binding energy calculation as a function of the energy offset $E_{\rm off}$ of Eq. (29). Horizontal line at -7.308 MeV corresponds to the value obtained in Ref. [17].

This simple kinematical argument may be made more stringent by investigating the various partial-wave contributions to the Schmidt norm of the three-body LS kernel. Writing the kernel of (14) as

$$K_{\beta\alpha}^{\Gamma I}(q',q;E+i0)=\sum_{\mu} V_{\beta\mu}^{\Gamma I}(q',q;E+i0)\Delta_{\mu\alpha}(E-\tfrac{3}{4}q^2+i0)\ , \tag{30}$$

its Schmidt norm is defined by

$$N_S^2=\mathrm{Tr}K^{\dagger}K=\sum_{\beta,\alpha}\int_0^{\infty}dq\int_0^{\infty}dq'(q'q|K_{\beta\alpha}^{\Gamma I}(q',q;E+i0)|)^2\ . \tag{31}$$

To see in some more detail the internal structure of all contributions for fixed q and fixed quantum number sets β and α, let us look at the simple case of S waves only; these contributions are then written explicitly as

$$\int_0^{\infty}dq'\left[q'q\left|\int_{-1}^{+1}dx\frac{W^{\eta'}(p_x',k';E_2')W^{\eta}(p_x,k;E_2)}{E-q^2-q'^2-qq'x+i0}\Delta^{\eta}(E-\tfrac{3}{4}q^2)\right|\right]^2\ . \tag{32}$$

Because of $E_2=E-\frac{3}{4}q^2$, fixed values of q correspond to a definite two-body subsystem energy and for p_x, one has

$$p_x=\sqrt{q'^2+\tfrac{1}{4}q^2+qq'x}$$

according to (20). If one now samples all contributions in the q' and x integrations of (32) for which this two-body momentum p_x is equal to a given, fixed value p, the result of this sampling procedure may be written as a function of E_2 and p,

$$n^{\eta'\eta}(E_2,p)=\left|\int_{-1}^{+1}dx\frac{W^{\eta'}(p',k';E_2')W^{\eta}(p,k;E_2)}{E_2-\frac{1}{4}q^2-q'^2+qq'x+i0}\Delta^{\eta}(E_2)q'q\right|^2\ , \tag{33}$$

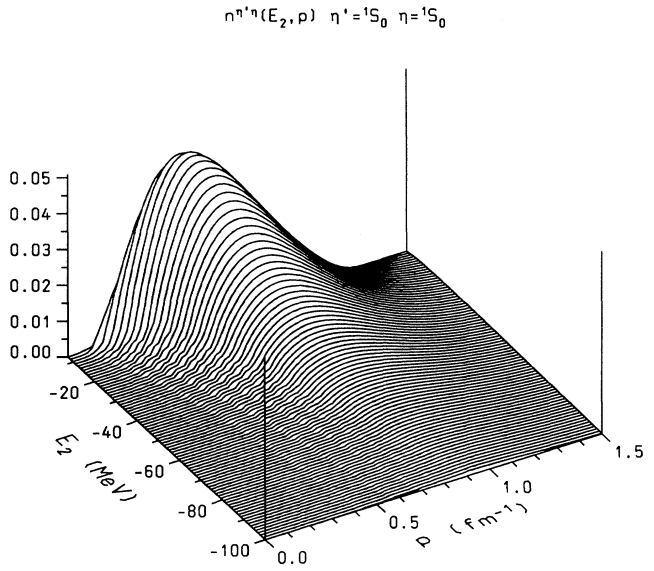

FIG. 2. Three-dimensional plot of Schmidt norm contribution, Eq. (33), at -7.3 MeV for subsystem transitions ${}^1S_0 \rightarrow {}^1S_0$. The channels spins are $K'=K=\frac{1}{2}$ and the channel angular momenta $L'=L=0$. The corresponding contour plot is shown in Fig. 3.

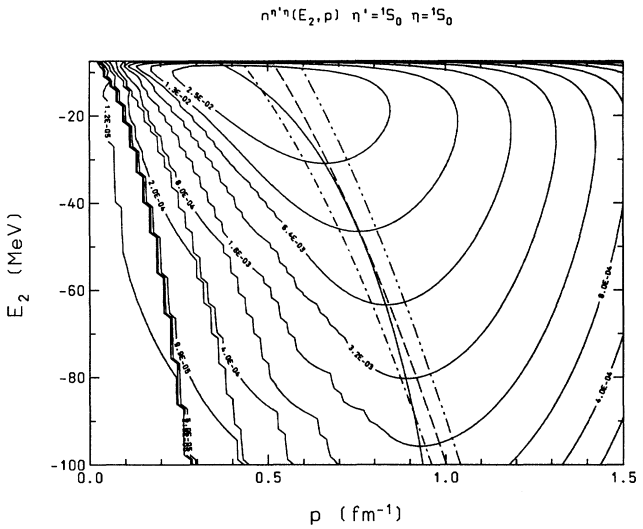

FIG. 3. Contour plot of Schmidt norm contribution, Eq. (33), at -7.3 MeV for subsystem transitions ${}^1S_0 \rightarrow {}^1S_0$. Figure 2 shows the corresponding 3D plot. Dashed-dotted, dashed, and dashed-double dotted lines depict Eq. (29) with energy offsets of 15, 25, and 35 MeV, respectively. Maximal contributions to the Schmidt norm are found along the solid line.

where q' is constrained by

$$q'=-\tfrac{1}{2}qx\pm\sqrt{\tfrac{1}{4}(qx)^2-\tfrac{1}{4}q^2+p^2}\ , \tag{34}$$

and p' and E'_2 are given by

$$p'=\sqrt{p^2+\tfrac{3}{4}q^2-\tfrac{3}{4}q'^2}\ , \tag{35}$$

$$E'_2=E-\tfrac{3}{4}q'^2\ , \tag{36}$$

respectively. The x integration in (33)—which is not to be confused with the x integration in (32)—ranges over intervals for which q' in (34) is positive; if both signs of the square root are possible, $n^{\eta'\eta}(E_2,p)$ contains the sum of the corresponding contributions. We recall here that (33) pertains to the S-wave case only. In general, for arbitrary partial waves, we will use the notation $n^{\beta\alpha}(E_2,p)$ with β and α given by (15). The detailed derivation of $n^{\beta\alpha}(E_2,p)$ is completely analogous to (33) and follows from (31) using (30) and (19). The various two-body partial-wave contributions are obtained by looking at the individual l and l' contributions in the corresponding sum of (19).

Choosing now the W-matrix parameter k as a function of the (negative) two-body subsystem energy E_2 such that it corresponds to the values p where $n^{\beta\alpha}(E_2,p)$ has dominant contributions, one has a criterion similar in spirit to the kinematic argument above but much more powerful in determining different functional forms for different two-body partial-wave contributions. From the construction, since one looks at contributions for fixed q, it is obvious that this pertains to the two-body channel within α, and not β. Since $n^{\beta\alpha}(E_2,p)$ describes transitions $\alpha\rightarrow\beta$, this procedure is not unique, but a comparison of transitions into different channels β allows one to infer optimized functional forms $k_{\hat{l}\hat{l}}(E_2)$ for $W^{\eta}_{\hat{l}\hat{l}}(p,k,E_2)$ fairly well. Our experience suggests that the dependence on the physical partial-wave index l is far more important than the one on the unphysical label $\hat{l}$; i.e., $k_{\hat{l}\hat{l}}(E_2)$ may be chosen as a constant with respect to $\hat{l}$ [with the corresponding dependence of $n^{\beta\alpha}(E_2,p)$ on $\hat{l}'$ and $\hat{l}$ being summed away according to the trace prescription of Eq. (31)].

Figure 2 shows a 3D plot of the Schmidt norm contributions $n^{\beta\alpha}(E_2,p)$ at the triton energy of -7.3 MeV for subsystem transitions ${}^1S_0\rightarrow{}^1S_0$, and the corresponding contour plot is given in Fig. 3. As can be seen in the latter plot, the functional form of (29) for offsets ranging between 15 and 35 MeV is very close to the actual maximal values. (For comparison of the corresponding binding energies, see Fig. 1.) For this case only negative energies E_2 below -7.3 MeV are of interest. For three-body scattering energies $E>0$, the W matrices are required at all negative two-body energies. In Figs. 4 and 5, we show the 3D and contour plots for the scattering energy of 10 MeV. We find that the behavior is very similar to the negative-energy cases of Figs. 2 and 3, except for small negative energies E_2. There we see from Fig. 5 that the maximum values of $k(E_2)$ tend to small values faster than prescribed by the kinematic criterion (29). In order to accommodate this behavior, we chose for $k(E_2)$ the functional form of the dashed-double dotted line in Fig. 5. For energies below the deuteron energy E_d, this corresponds to Eq. (29) with $E_{\rm off}=35$ MeV and between $E_2=E_d$ and $E_2=0$, we simply pull down $k(E_2)$ smoothly to zero at $E_2=0$. Since we find a very similar average behavior also for the coupled ${}^3S_1$-${}^3D_1$ channel, we use the functional form from Fig. 5 for this case, too.

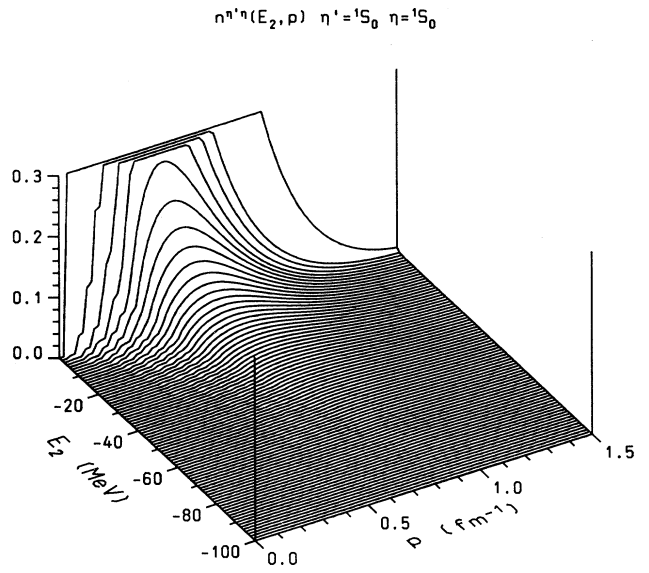

FIG. 4. Same as Fig. 2, for the scattering energy of 10 MeV. The corresponding contour plot is shown in Fig. 5.

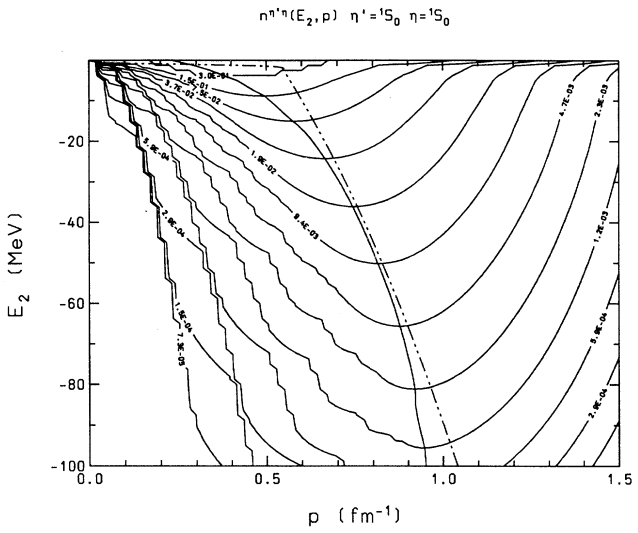

FIG. 5. Same as Fig. 3, for the scattering energy of 10 MeV. Figure 4 shows the corresponding 3D plot. Maximal contributions to the Schmidt norm are found along the solid line; the dashed-double dotted line corresponds to our choice of $k(E_2)$.

For seven-channel three-body observables we find that the detailed functional form of pulling down the values of k to zero has negligible influence on the final results. In this respect, it should also be noted that the essential aspects of Figs. 2–5 do not change if different (reasonable) functions $k(E_2)$ are employed in calculating $n^{\beta\alpha}(E_2,p)$. In other words, the norm criterion itself is largely independent of $k(E_2)$ and allows one to choose $k(E_2)$ in one single step, without having to go through several iterative stages.

While the actual numerical calculation of optimized functional forms for $k(E_2)$ according to the procedure just described requires only negligible computing time compared to the solution of the full three-body AGS equations (14), its development and testing against alternative possibilities used up quite a bit of the granted CRAY computing time. As a consequence, we could not fully implement the Schmidt norm criterion for all subsystem partial waves. As a compromise, we chose the same functional form as in Fig. 5 for all two-body partial waves considered in the present work. While we find that this is a very good choice for the seven-channel case using ${}^1S_0$ and ${}^3S_1$-${}^3D_1$ and a good average choice for other partial waves, we do not consider it as being fully optimized yet. As an example of the latter point, we present in Figs. 6 and 7 three-dimensional and contour plots for the ${}^3P_2$ subsystem. One clearly sees that our choice for $k(E_2)$ is inadequate to describe the dominant features of this partial wave in detail; it essentially only skims the slopes of some of the peaks and almost entirely misses the largest of these peaks. As a result, some of the observables reported in the next section, in particularly those depending very sensitively on certain P-wave contributions, are expected to improve if one uses more refined functional forms for $k_{ll'}(E_2)$ in the P waves.

We emphasize here that our criterion is a *three-body* criterion, i.e., we optimize our two-body input with respect to the three-body kernel. Conventional *two-body* norm criteria cannot provide more than an indication of the quality of the approximation in the context of the three-body problem. A genuine practical criterion must by necessity be a three-body criterion.

IV. NUMERICAL RESULTS

The numerical solution of the W-matrix equation (2) can be done without any problems for all energies since it is nonsingular. To provide an accurate input for the AGS equations (14), we require the half-on-shell solutions of (2) on a discrete energy mesh of 105 points where 65 of these points are at negative energies. The corresponding solutions of (2) are obtained on a momentum mesh of 120 points. The resulting W matrices of dimension 105×120 then provide the basis for a two-dimensional spline representation which allows a very accurate calculation at arbitrary energies and momenta. As mentioned already, as input we use the Paris potential [5]. Since, by construction, the separable W-matrix representation (6) is exact half on-shell, our approximate input reproduces, of course, all of the on-shell data of the Paris potential.

In solving the AGS equation (14) numerically, we used essentially the same methods as discussed in Ref. [1]. We solved Eq. (14) on the real axis by expanding the solutions into cubic B splines [18]. The logarithmic singularity originating from the x integration of (19) was treated by standard subtraction techniques. We used at least 16 mesh points for the x integration and at least 50 cubic B splines to expand the unknown solutions. The necessary momentum integrations of the kernel (14) over the given spline functions were done with more than 130 mesh points. *We emphasize that the relative simplicity of the*

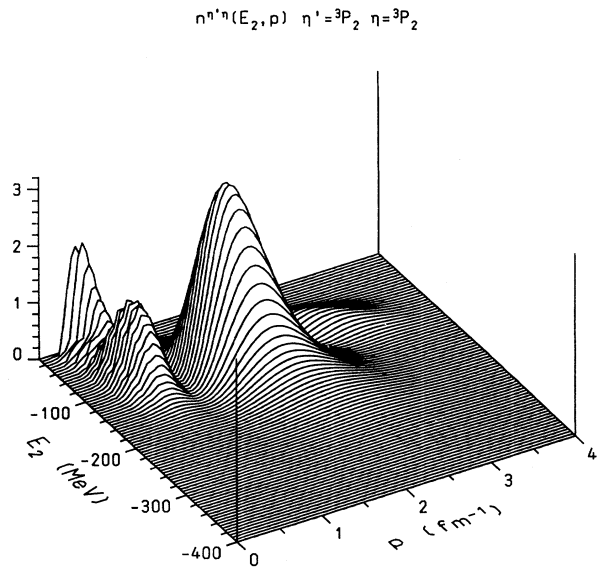

FIG. 6. Three-dimensional plot of Schmidt norm contribution for subsystem transitions ${}^3P_2 \rightarrow {}^3P_2$. The channels spins are $K'=K=\frac{3}{2}$ and the channel angular momenta $L'=L=1$. The corresponding contour plot is shown in Fig. 7.

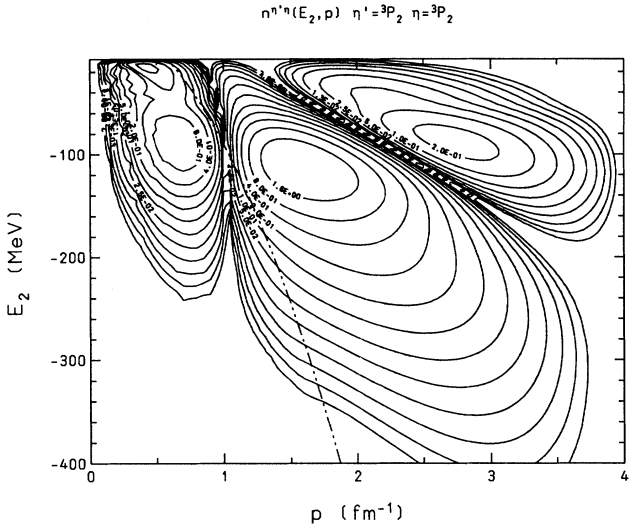

FIG. 7. Contour plot of Schmidt norm contribution for subsystem transitions ${}^3P_2 \rightarrow {}^3P_2$. The corresponding 3D plot is given in Fig. 6. The dashed-double dotted line shows our choice for $k(E_2)$ (cf. Fig. 5).

three-nucleon equations (14) afforded by the W-matrix approach allowed us to consistently choose the size of our integration and spline meshes on the safe side. Hence, the numerical accuracy of the on-shell solution of the AGS equation (14) is better than 1%. (For further technical details, see Ref. [11].)

In Figs. 8–25 we present our results for an almost complete set of neutron-deuteron observables at a neutron laboratory energy of 10 MeV (solid lines); the definitions of the respective observables are taken from Ref. [19]. For comparison, we also give the theoretical direct-integration results of Witała *et al.* [7] (dashed lines). Since neutron-deuteron data are not available, we show experimental proton-deuteron data [20] at the same energy. The figures are the results for two different input sets. The respective parts (a) of all Figures 8–25 correspond to "small" input comprising two-body angular momenta $J^\pi \leq 1^+$ (i.e., the seven-channel problem with ${}^1S_0$ and ${}^3S_1$-${}^3D_1$), while parts (b) are based on the "large" input with $J \leq 2$ (i.e., 34 contributing two-body channels). In our results (solid lines), the maximal three-body total angular momentum is $\Gamma = \frac{19}{2}$ in both cases; contributions from higher Γ are negligible.

As can be seen from the plots, the observables obtained with small input [Figs. 8(a)–25(a)] are of the same quality as results of other solution algorithms [7,8]. For large input [Figs. 8(b)–25(b)], in view of the not quite optimized P-wave input, we still expect a possible improvement in the findings of Figs. 8(b)–12(b) and 14(b) if one uses better functional forms $k(E_2)$ for the P waves. The neutron and deuteron vector analyzing powers A_y (Fig. 8) and iT_{11} (Fig. 9), respectively, are particularly sensitive to variations of the P-wave input. The differences between our results (solid lines) and those of Ref. [7] (dashed lines) may be attributed to this fact. For all other observables, however, we do not expect any appreciable

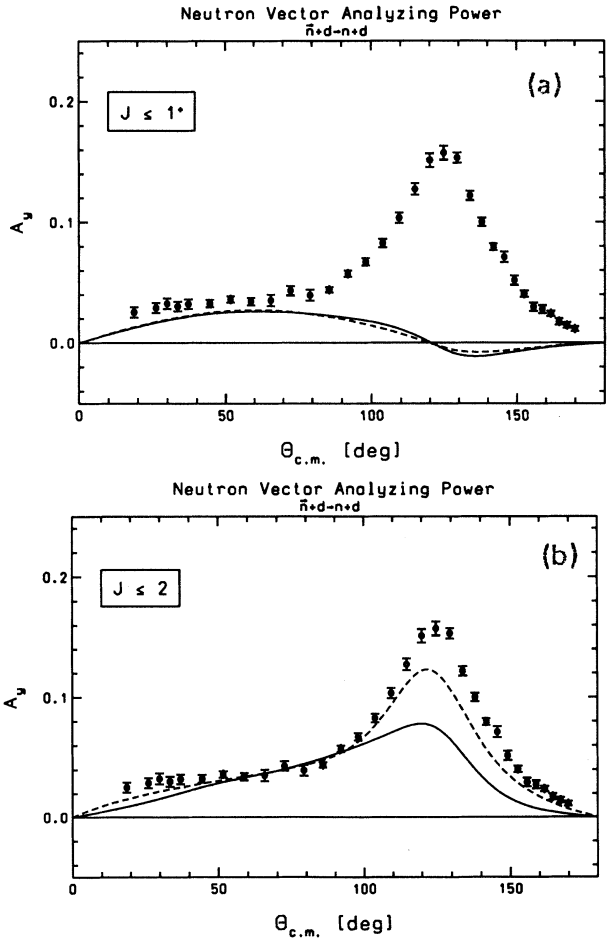

FIG. 8. Neutron vector analyzing power A_y for (a) small ($J^\pi \leq 1^+$) and (b) large ($J \leq 2$) two-body input. Solid lines: this work; dashed lines: Ref. [7] (see also remark at the end of Sec. IV); experimental proton-deuteron data: Ref. [20].

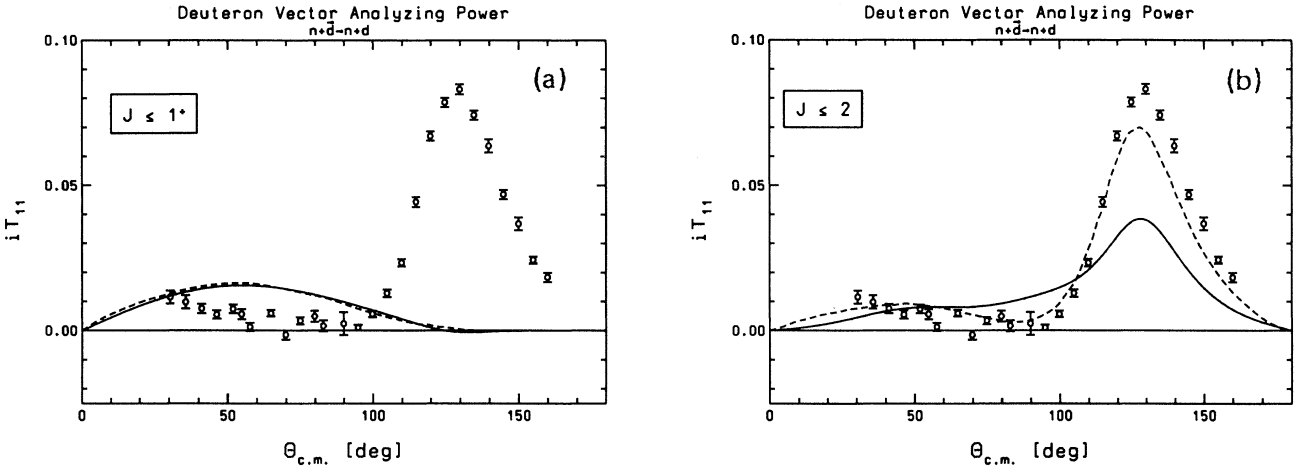

FIG. 9. Deuteron vector analyzing power iT_{11} for (a) small ($J^{\pi} \leq 1^{+}$) and (b) large ($J \leq 2$) two-body input. Line styles as in Fig. 8.

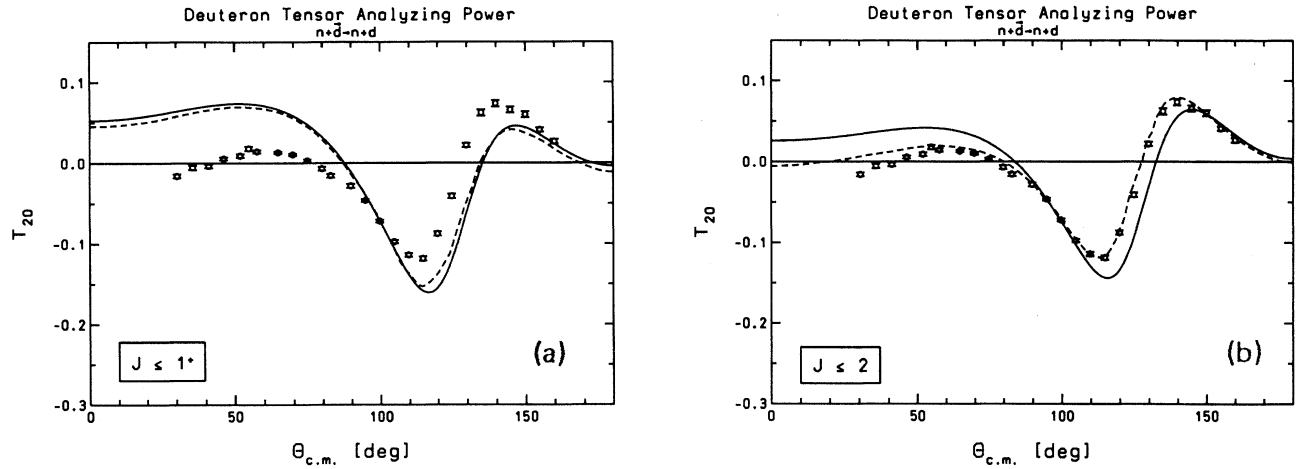

FIG. 10. Deuteron tensor analyzing power T_{20} for (a) small ($J^{\pi} \leq 1^{+}$) and (b) large ($J \leq 2$) two-body input. Line styles as in Fig. 8.

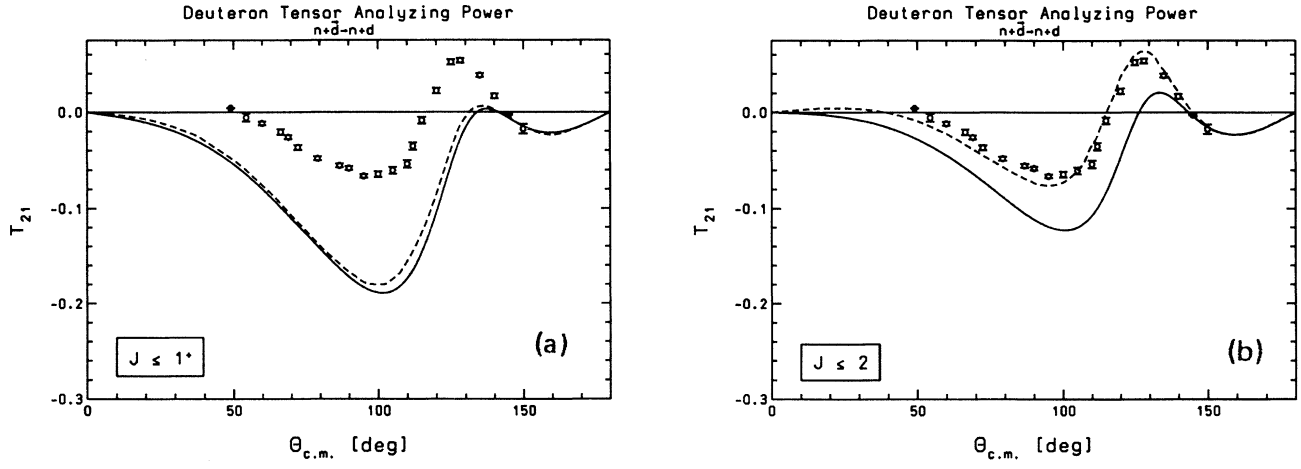

FIG. 11. Deuteron tensor analyzing power T_{21} for (a) small and (b) large ($J \leq 2$) two-body input. Line styles as in Fig. 8.

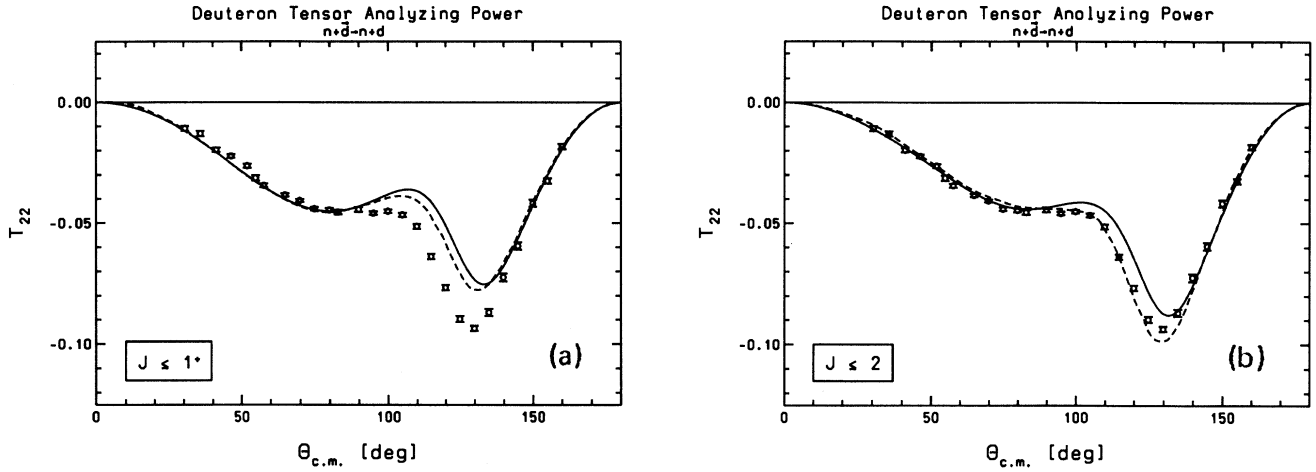

FIG. 12. Deuteron tensor analyzing power T_{22} for (a) small ($J^{\pi} \leq 1^{+}$) and (b) large ($J \leq 2$) two-body input. Line styles as in Fig. 8.

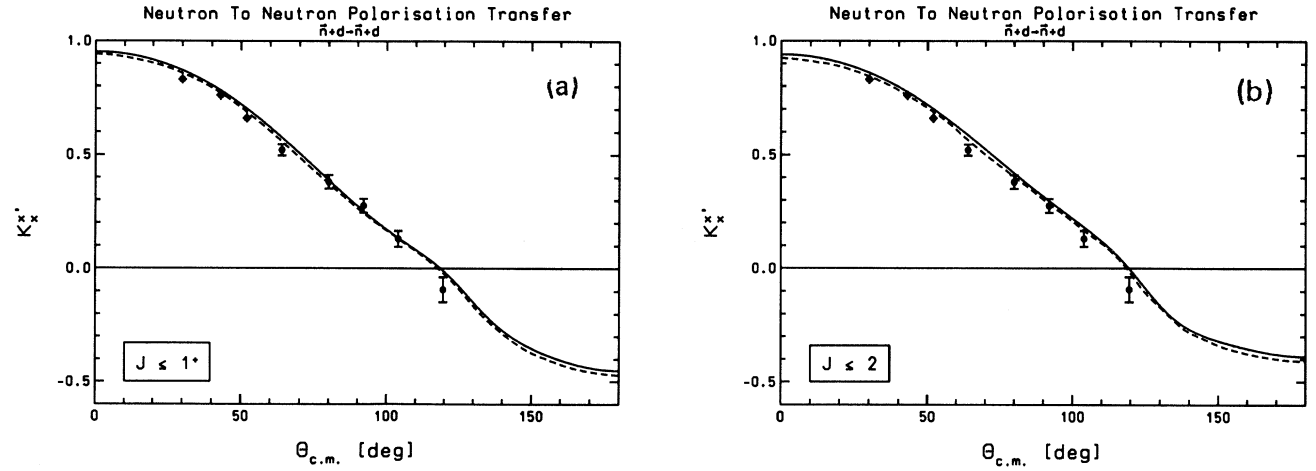

FIG. 13. Neutron-to-neutron polarization transfer $K_x^{x'}$ for (a) small ($J^{\pi} \leq 1^{+}$) and (b) large ($J \leq 2$) two-body input. Line styles as in Fig. 8.

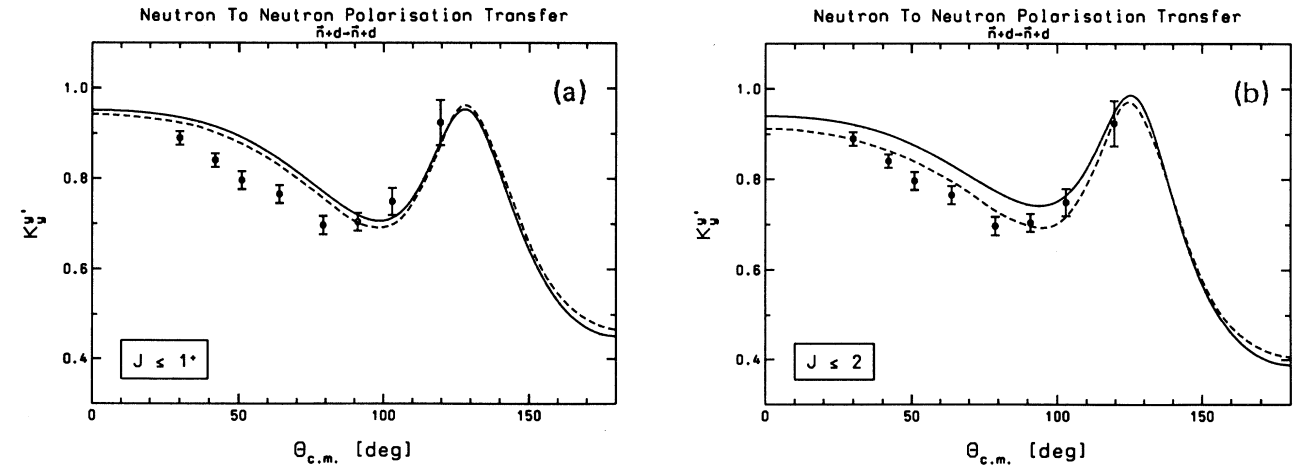

FIG. 14. Neutron-to-neutron polarization transfer $K_y^{y'}$ for (a) small ($J^{\pi} \leq 1^{+}$) and (b) large ($J \leq Z$) two-body input. Line styles as in Fig. 8.

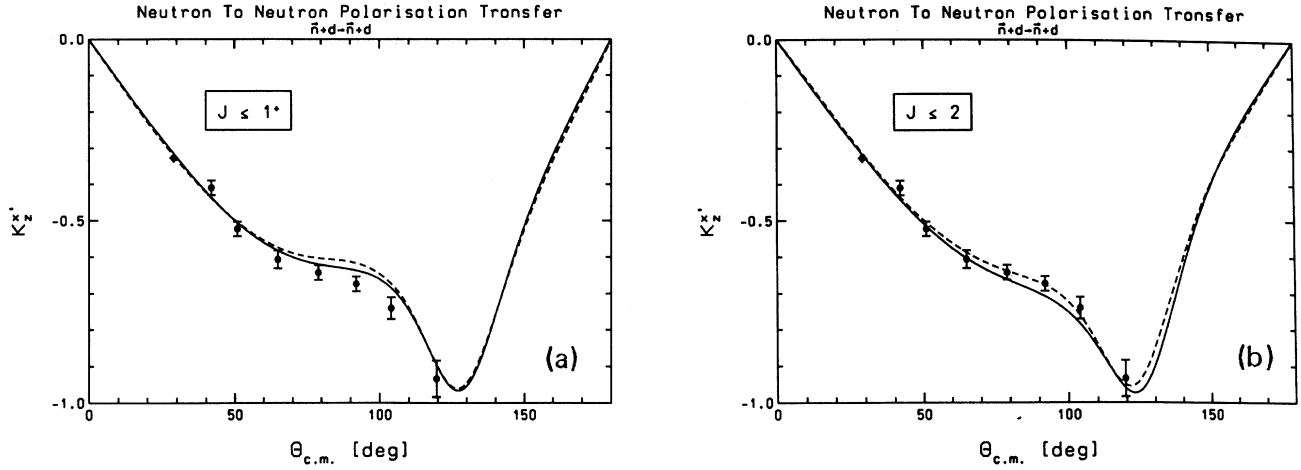

FIG. 15. Neutron-to-neutron polarization transfer $K_z^{x'}$ for (a) small ($J^\pi \leq 1^+$) and (b) large ($J \leq 2$) two-body input. Line styles as in Fig. 8.

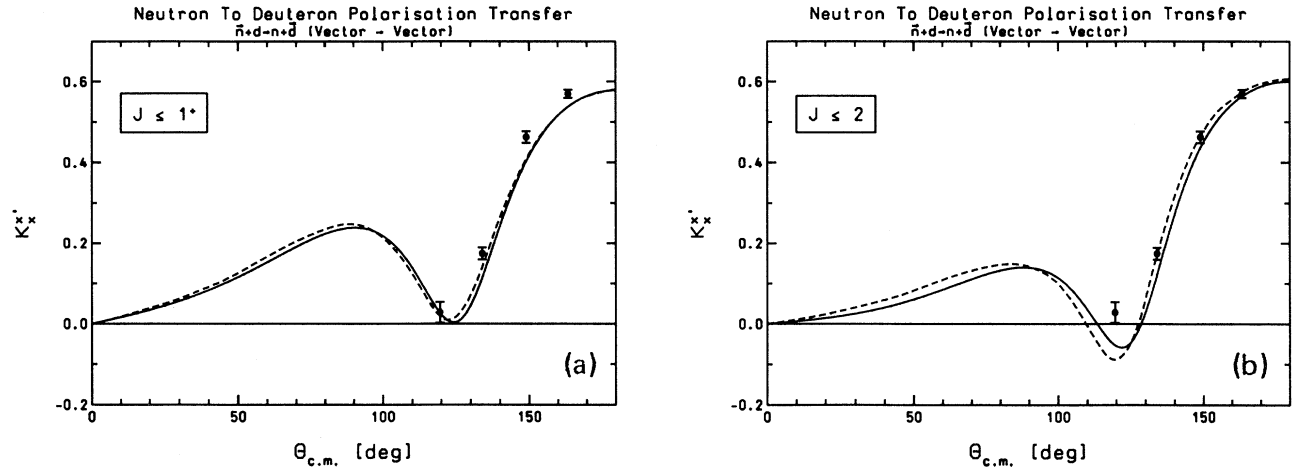

FIG. 16. Neutron-to-deuteron polarization transfer $K_x^{x'}$ for (a) small ($J^\pi \leq 1^+$) and (b) large ($J \leq 2$) two-body input. Line styles as in Fig. 8.

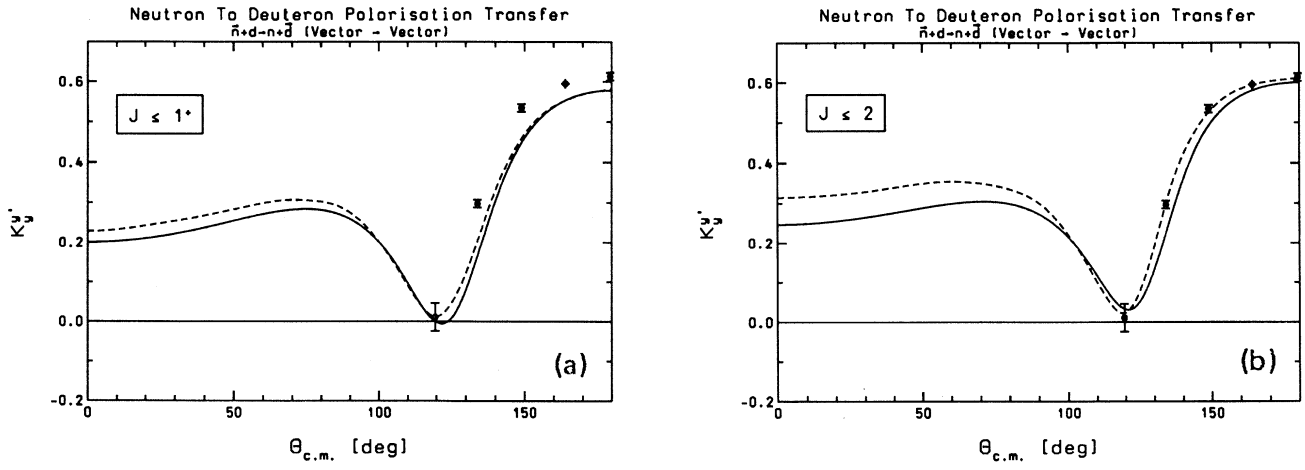

FIG. 17. Neutron-to-deuteron polarization transfer $K_y^{y'}$ for (a) small ($J^\pi \leq 1^+$) and (b) large ($J \leq 2$) two-body input. Line styles as in Fig. 8.

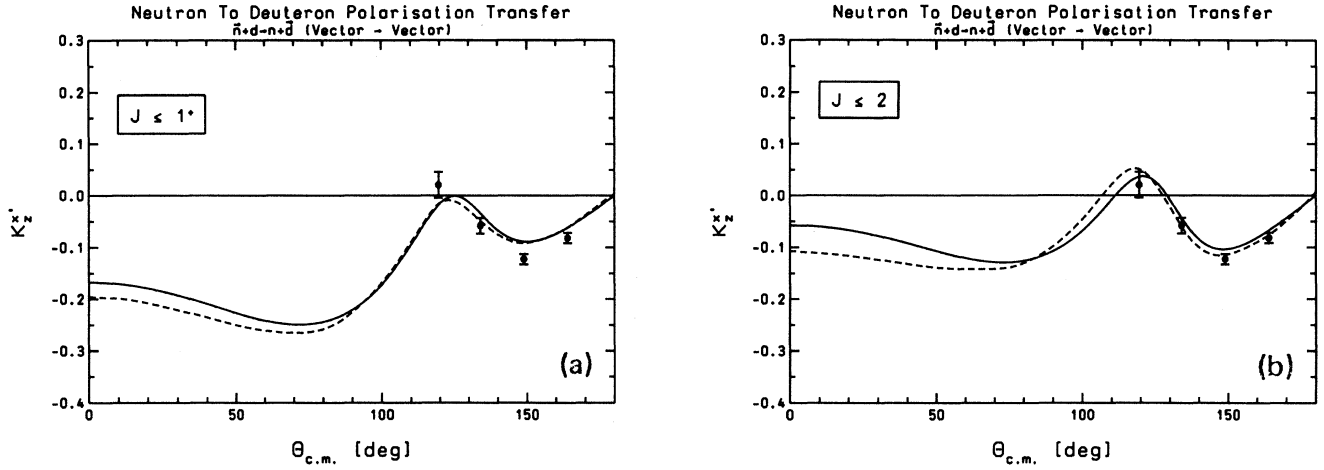

FIG. 18. Neutron-to-deuteron polarization transfer $K_z^{x'}$ for (a) small ($J^\pi \leq 1^+$) and (b) large ($J \leq 2$) two-body input. Line styles as in Fig. 8.

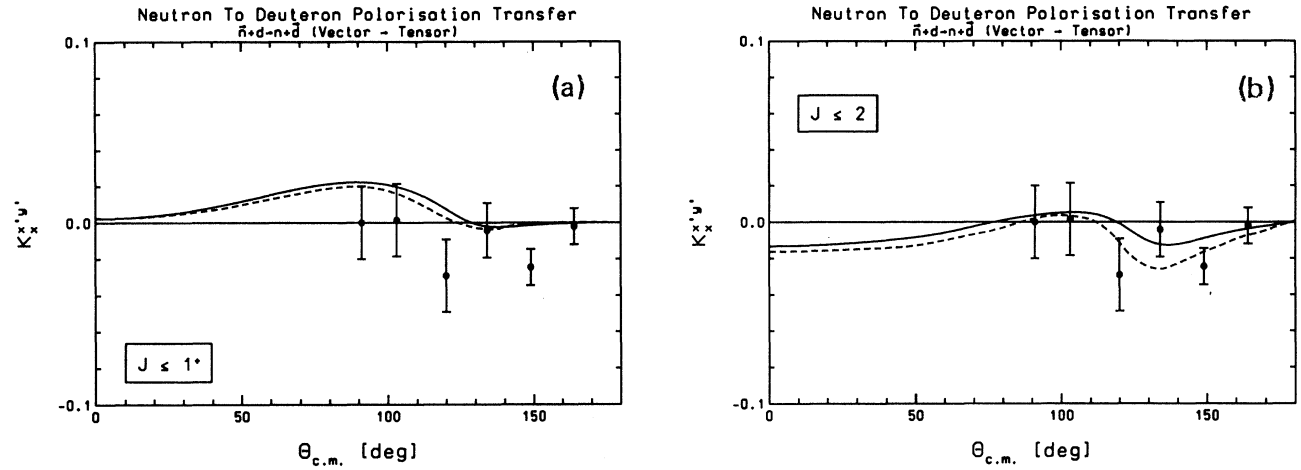

FIG. 19. Neutron-to-deuteron polarization transfer $K_x^{x'y'}$ for (a) small ($J^\pi \leq 1^+$) and (b) large ($J \leq 2$) two-body input. Line styles as in Fig. 8.

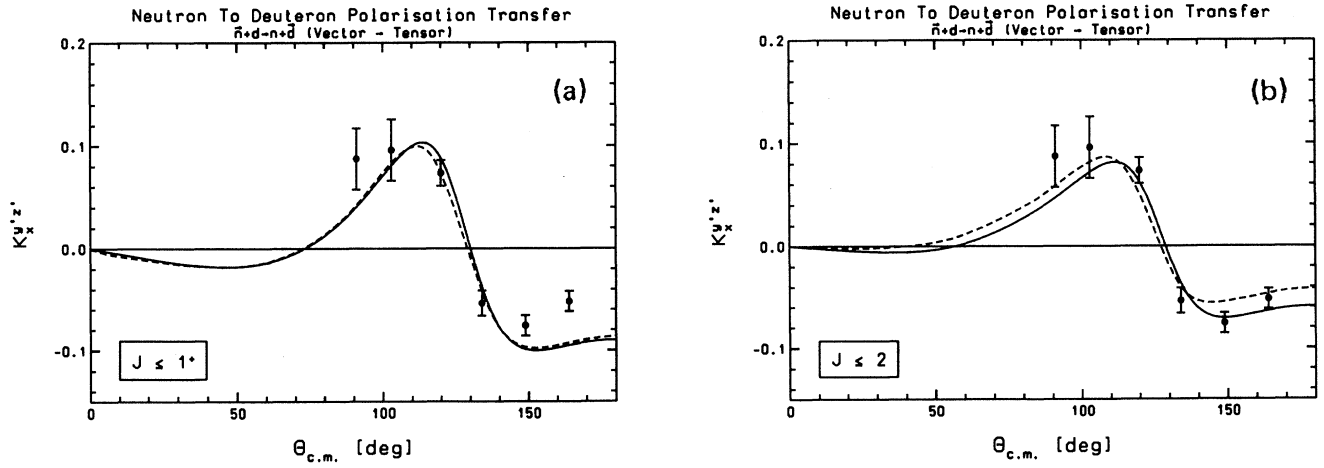

FIG. 20. Neutron-to-deuteron polarization transfer $K_x^{y'z'}$ for (a) small ($J^\pi \leq 1^+$) and (b) large ($J \leq 2$) two-body input. Line styles as in Fig. 8.

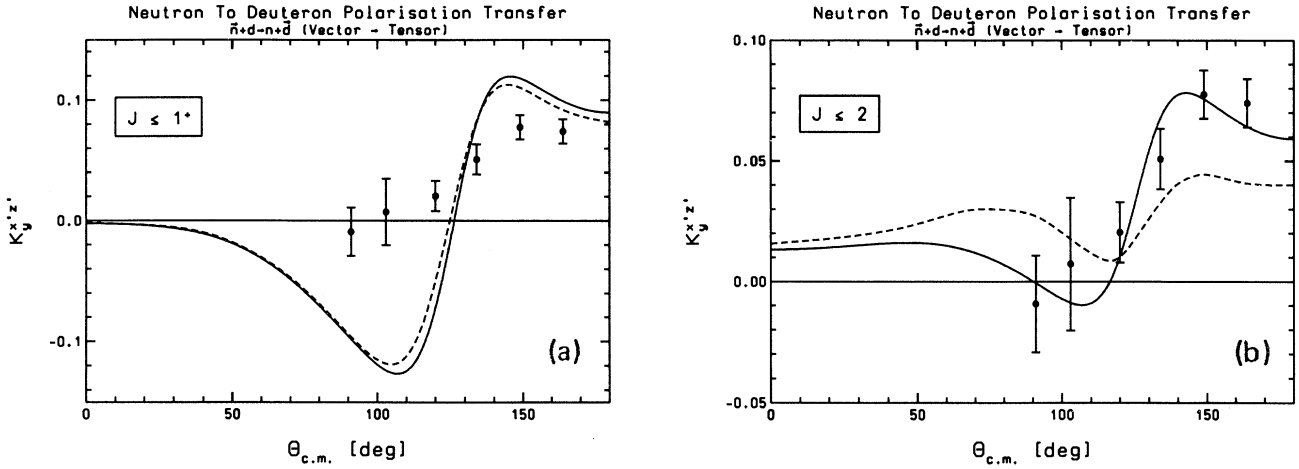

FIG. 21. Neutron-to-deuteron polarization transfer $K_y^{x'z'}$ for (a) small ($J^\pi \leq 1^+$) and (b) large ($J \leq 2$) two-body input. Line styles as in Fig. 8.

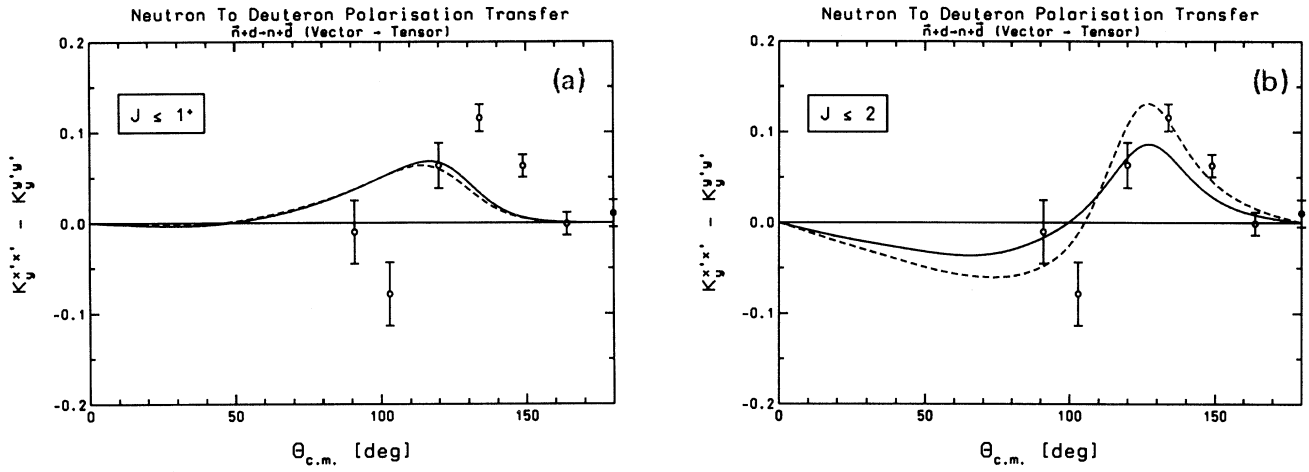

FIG. 22. Neutron-to-deuteron polarization transfer $K_y^{x'x'} - K_y^{y'y'}$ for (a) small ($J^\pi \leq 1^+$) and (b) large ($J \leq 2$) two-body input. Line styles as in Fig. 8.

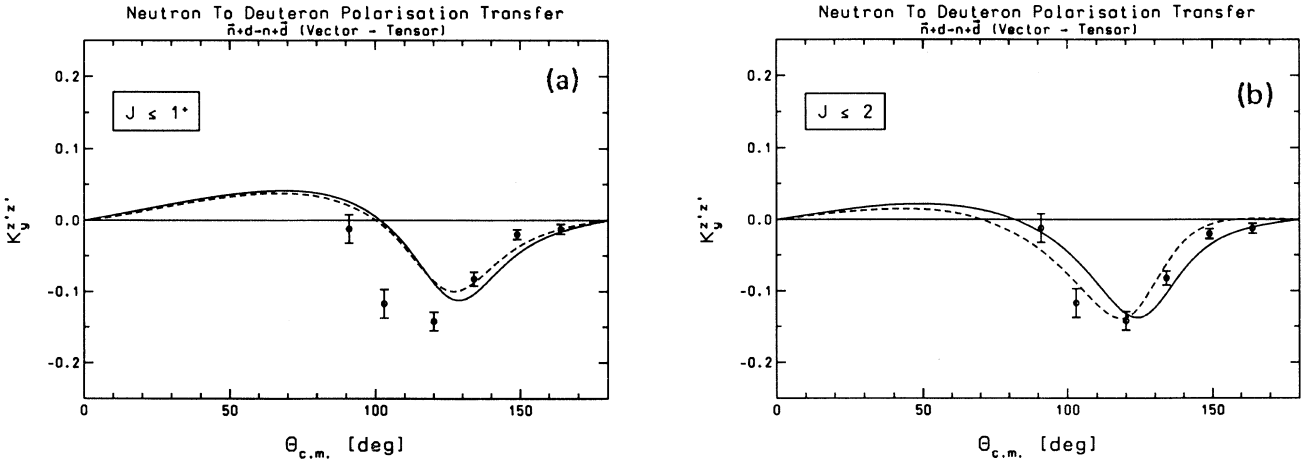

FIG. 23. Neutron-to-deuteron polarization transfer $K_y^{z'z'}$ for (a) small ($J^\pi \leq 1^+$) and (b) large ($J \leq 2$) two-body input. Line styles as in Fig. 8.

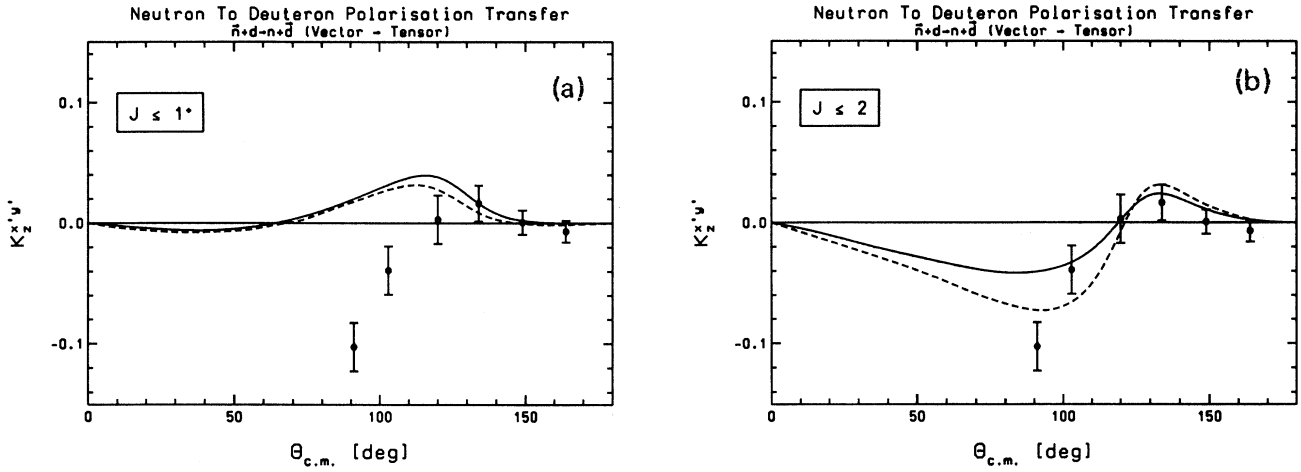

FIG. 24. Neutron-to-deuteron polarization transfer $K_z^{x'y'}$ for (a) small ($J^\pi \leq 1^+$) and (b) large ($J \leq 2$) two-body input. Line styles as in Fig. 8.

changes even if we improve our present P-wave input. As can be seen from the figures, for those insensitive observables our results are in good agreement with those of Ref. [7], with the exception of the neutron-to-deuteron polarization transfer $K_y^{x'y'}$ of Fig. 21(b). In our experience, this observable is not very sensitive to a variation of the P-wave input, yet our 34-channel results are quite different from, and in better agreement with the experimental data than, those of Witała *et al.* [7] (It should be mentioned in this context that the curves of the calculations of Witała *et al.* were extracted from plots; numerical values of their results were not available to us. Some of the differences of our results to those of Witała *et al.* may be attributed to our errors in reading off the plotted results of Ref. [7], i.e., practically all differences between the small-input results shown in Fig. 8(a)–25(a) may be understood in this way.)

V. CONCLUSIONS

In order to discuss the particular merits of the W-matrix approach in somewhat more detail, let us first compare it with one of the most successful separable expansion methods, the Ernst-Shakin-Thaler (EST) expansion [9]. Its convergence when employed for the Paris potential was studied in Ref. [8]. Using the two-nucleon $^1S_0$ and the $^3S_1$-$^3D_1$ partial waves as examples of uncoupled and coupled partial waves, respectively, it was found [8] that one requires at least rank-5 and rank-6 approximations, respectively, to obtain reliable approximations of the two-body on-shell data for the Paris potential. In the language of Ref. [8], ranks 5 or 6 correspond to 25 or 36 terms in the respective expansions. The W-matrix approximation of Eq. (6), by comparison, requires only 1 or 4 terms, respectively, corresponding to rank 1 or tank 2.

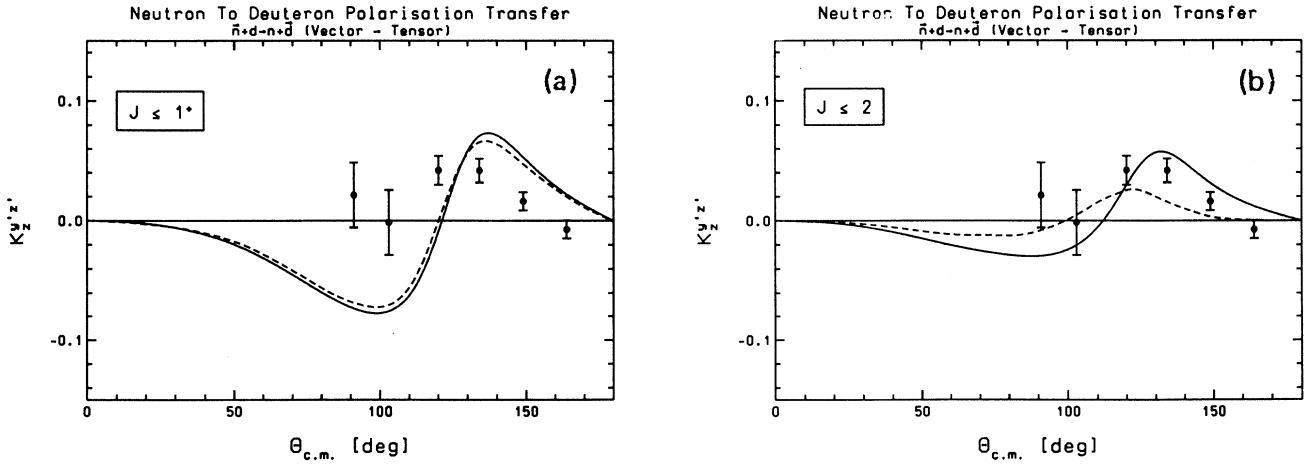

FIG. 25. Neutron-to-deuteron polarization transfer $K_z^{y'z'}$ for (a) small ($J^\pi \leq 1^+$) and (b) large ($J \leq 2$) two-body input. Line styles as in Fig. 8.

For the half-on-shell T-matrix elements, this provides an analytically exact description. Optimizing, furthermore, the still open parameter function $k(E_2)$ according to the procedure of Sec. III, the corresponding three-body seven-channel W-matrix results are seen to be of the same quality as those of other calculations [7,8]. As an—admittedly somewhat crude—measure of the required numerical work for both approaches, one may use the respective sizes of the integral-equation kernel matrices, since this, in our experience, determines to a large part the necessary computational resources, in particular, the computing time. Using the same mesh sizes for the momentum integrations, the difference between 1 and 25 or 4 and 36 terms in the respective expansions implies that for a five-channel calculation in the EST approach one needs to calculate about a factor of 10 more matrix elements. This factor increases with an increasing number of channels.

Comparing our approach to a direct two-dimensional discretization [7], our estimates for the most basic problem, the five-channel problem, indicate that the number of matrix elements for the latter is at least a factor of 100 larger. Again, this factor increases drastically with an increasing number of channels. In making these estimates we emphasize that we compare here our generous mesh sizes with the relatively small ones gives in Ref. [7], despite the fact that we consider the latter inadequate to obtain the overall numerical accuracy claimed there.

In this context, let us add a comment of a more general nature. In a problem as complicated as the nuclear three-body problem, one is always faced with the danger of running out of computational resources. However, if sacrifices in accuracy have to be made, they ought to be made where they hurt least, if possible. It is the nature of elastic nucleon-deuteron scattering that it can be understood very well as an effective two-body problem in which the dominant dynamical mechanism is that of a single nucleon interacting with a composite two-nucleon subsystem. It seems obvious, therefore—and our experience bears out this prejudice—that one should not make any compromise in describing the dynamics of this relative motion of the spectrator nucleon, because a too- crude approximation there will have direct and immediate consequences on the final results. If approximations have to be made, they ought to be made within the two-nucleon subsystem where their bearing on the elastic nucleon-deuteron observables is less direct and averaged out to a very large degree by the way effective two-body matrix elements are formed, where subsystem information is integrated away. In view of the fact that the degree of coupling of the three-body equations within the W-matrix approach is exactly identical to what is prescribed by angular momentum decomposition, without any additional couplings due to an unspecific separable expansion, and without the additional subsystem integration of a direct-integration approach, the W-matrix method constitutes a solution algorithm where the size for the resulting system of linear equations is as small as is possible according to the quantum number structure of the problem. It is for this reason that we can afford to make no compromise in choosing the corresponding integration mesh size and solve the effective two-body equation (14) as accurately as possible. In this respect the W-matrix approach provides a numerically very cost-effective and reliable method of calculating three-body scattering data even for realistic potentials.

Summarizing, we have presented here a numerical solution of the three-nucleon AGS equations within the framework of the W-matrix approach [4]. While previous implementations [1,2] of this method were restricted to the simple W-wave Malfliet-Tjon potentials [3], the present investigation is based on the Paris potential [5], considered to be one of the most realistic two-nucleon interactions. The results reported here corroborate the previous findings, namely that the W-matrix approach provides a very efficient means of obtaining high-quality solutions for three-nucleon processes. This conclusion is notwithstanding the fact that at present, for lack of computing time, we have only been able to optimize the two-body input for the $^1S_0$ and $^3S_1$-$^3D_1$ two-body partial waves. Preliminary work concerning the optimization of other partial waves, however, has been carried out already and we are confident that the corresponding three-nucleon results will be of similar quality as the seven-channel results with $^1S_0$ and $^3S_1$-$^3D_1$ input.

ACKNOWLEDGMENT

One of the authors (H.H.) would like to thank the Physikalisches Institut der Universität Bonn for financial support and for the warm hospitality during the time when this manuscript was written. His work was supported in part by the U.S. Department of Energy, Grant No. DE-FG05-86-ER40270. Moreover, we thank Professor W. Grüebler for providing us with experimental data [20] and the HLRZ Jülich for a grant of CRAY computing time.

APPENDIX

In calculating the spin-isospin recoupling coefficient $U^{\Gamma I}_{\beta\alpha}(H,h)$ of Eq. (19) we followed the conventions of Edmonds [21]; the notation is very similar to the one by Doleschall [22]. The coefficients may be decomposed as

$$U^{\Gamma I}_{\beta\alpha}(H,h)=\Gamma_{\beta\alpha}(H,h)I_{\beta\alpha}\ , \tag{A1}$$

where β and α have the same meaning as in Eq. (15). The isospin factor $I_{\beta\alpha}$ is given by

$$I_{\beta\alpha}=(-1)^T\sqrt{(2T+1)(2T'+1)}\begin{Bmatrix}\frac{1}{2} & \frac{1}{2} & T'\\ \frac{1}{2} & I & T\end{Bmatrix}\ , \tag{A2}$$

and for the spin factor $\Gamma_{\beta\alpha}(H,h)$ one has

$$\Gamma_{\beta\alpha}(H,h)=\tfrac{1}{2}\sum_{f=f_{\min}}^{f_{\max}}[1+(-1)^{l'+f-h}]E^{\Gamma}_{\beta\alpha}[H,\tfrac{1}{2}(f+l'-h),\tfrac{1}{2}(f-l'+h)]\ , \tag{A3}$$

where $f_{\min}=|l'-h|$ and $f_{\max}=l+l'-|l-h|$ and

$$E^{\Gamma}_{\beta\alpha}(H,f',f)=(-1)^{l'+L+L'}(\tfrac{1}{2})^{f+f'}(2l+1)(2l'+1)(2H+1)\left[(2L+1)(2L'+1)\begin{Bmatrix}2l\\2f\end{Bmatrix}\begin{Bmatrix}2l'\\2f'\end{Bmatrix}\right]^{1/2}$$
$$\times\sum_{h,h'}(2h+1)(2h'+1)\begin{Bmatrix}L&f&h\\0&0&0\end{Bmatrix}\begin{Bmatrix}h&l'-f'&H\\0&0&0\end{Bmatrix}\begin{Bmatrix}L'&f'&h'\\0&0&0\end{Bmatrix}\begin{Bmatrix}h'&l-f&H\\0&0&0\end{Bmatrix}$$
$$\times\sum_{F}(2F+1)\begin{Bmatrix}l-f&f&l\\L&F&h\end{Bmatrix}\begin{Bmatrix}l'-f'&f'&l'\\L'&F&h'\end{Bmatrix}\begin{Bmatrix}l'-f'&f&h\\l-f&H&h'\end{Bmatrix}C^{\Gamma}_{\beta\alpha}(F)\,, \tag{A4}$$

with

$$C^{\Gamma}_{\beta\alpha}(F)=(-1)^{2\Gamma+1+S'}\sqrt{(2J+1)(2J'+1)(2K+1)(2K'+1)(2S+1)(2S'+1)}$$
$$\times\sum_{G}(2G+1)\begin{Bmatrix}\frac{1}{2}&\frac{1}{2}&S'\\\frac{1}{2}&G&S\end{Bmatrix}\begin{Bmatrix}l&S&J\\\frac{1}{2}&K&G\end{Bmatrix}\begin{Bmatrix}G&l&K\\L&\Gamma&F\end{Bmatrix}\begin{Bmatrix}l'&S'&J'\\\frac{1}{2}&K'&G\end{Bmatrix}\begin{Bmatrix}G&l'&K'\\L'&\Gamma&F\end{Bmatrix}. \tag{A5}$$

Here, ( ) and { } are $3j$ and $6j$ symbols, respectively.

[1] E. A. Bartnik, H. Haberzettl, Th. Januschke, U. Kerwath, and W. Sandhas, Phys. Rev. C **36**, 1678 (1987).

[2] T. N. Frank, H. Haberzettl, Th. Januschke, U. Kerwath, and W. Sandhas, Phys. Rev. C **38**, 1112 (1988).

[3] R. A. Malfliet and J. A. Tjon, Nucl. Phys. **A127**, 161 (1969); Ann. Phys. (N.Y.) **61**, 425 (1970).

[4] E. A. Bartnik, H. Haberzettl, and W. Sandhas, Phys. Rev. C **34**, 1520 (1986); H. Haberzettl, *ibid*, **40**, 1147 (1989).

[5] M. Lacombe, B. Loiseau, J. M. Richard, R. Vinh Mau, J. Côté, P. Pirès, and R. de Tourreil, Phys. Rev. C **21**, 861 (1980).

[6] E. O. Alt, P. Grassberger, and W. Sandhas, Nucl. Phys. **B2**, 167 (1967); W. Sandhas, Acta Phys. Austriaca Suppl. **IX**, 57 (1972).

[7] H. Witała, T. Cornelius, and W. Glöckle, Few Body Systems **3**, 123 (1988); H. Witała, W. Glöckle, and T. Cornelius, Nucl. Phys. **A491**, 157 (1989).

[8] J. Haidenbauer and W. Plessas, Phys. Rev. C **27**, 63 (1983); J. Haidenbauer and Y. Koike, *ibid*. **34**, 1187 (1986).

[9] D. J. Ernst, C. M. Shakin, and R. M. Thaler, Phys. Rev. C **8**, 46 (1973); **9**, 1780 (1974).

[10] Chr. von Ferber, W. Sandhas, and H. Haberzettl, Phys. Rev. C **40**, 1923 (1989).

[11] Th. Januschke, Ph.D. thesis, BONN-IR-90-52, Universität Bonn, 1990.

[12] A. Conrads-Frank, T. N. Frank, H. Haberzettl, and U. Kerwath, unpublished.

[13] S. Weinberg, Phys. Rev. **130**, 776 (1963); **131**, 440 (1963).

[14] B. F. Gibson, B. C. Pearce, G. L. Payne, Phys. Rev. C **40**, 2877 (1989).

[15] H. Haberzettl and U. Kerwath, Phys. Rev. C **43**, 2895 (1991).

[16] Ch. Hajduk and P. U. Sauer, Nucl. Phys. **A369**, 321 (1981).

[17] J. L. Friar, B. F. Gibson, and G. L. Payne, Phys. Rev. C **37**, 2869 (1988).

[18] L. L. Schumaker, *Spline Functions: Basic Theory* (Wiley, New York, 1981).

[19] G. G. Ohlsen, Rep. Prog. Phys. **35**, 717 (1972).

[20] F. Sperisen, W. Grüebler, V. König, P. A. Schmelzbach, K. Elsener, B. Jenny, C. Schweizer, J. Ulbricht, and P. Doleschall, Nucl. Phys. **A422**, 81 (1984).

[21] A. R. Edmonds, *Angular Momentum in Quantum Mechanics* (Princeton University Press, Princeton, NJ, 1957).

[22] P. Doleschall, Nucl. Phys. **A201**, 264 (1973).